AGU PUBLICATIONS

Geophysical Research Letters

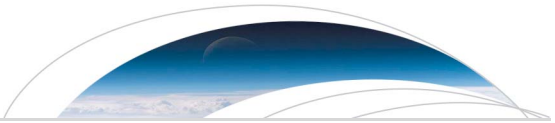

RESEARCH LETTER
10.1002/2015GL065095

Key Points:
- Model capable in reproducing realistic MJO is used for MJO projection
- Global warming enhances MJO
- Mutual reinforcement of thermodynamic and dynamic factors for stronger tilting

Supporting Information:
- Supporting Information S1
- Figure S1
- Figure S2
- Figure S3
- Figure S4
- Figure S5
- Table S1

Correspondence to:
C.-W. J. Chang,
c.june.chang@gmail.com

Citation:
Chang, C.-W. J., W.-L. Tseng, H.-H. Hsu, N. Keenlyside, and B.-J. Tsuang (2015), The Madden-Julian Oscillation in a warmer world, *Geophys. Res. Lett.*, *42*, 6034–6042, doi:10.1002/2015GL065095.

Received 25 JUN 2015
Accepted 6 JUL 2015
Accepted article online 7 JUL 2015
Published online 31 JUL 2015

The copyright line for this article was changed on 23 SEP 2015 after original online publication.

©2015. The Authors.
This is an open access article under the terms of the Creative Commons Attribution-NonCommercial-NoDerivs License, which permits use and distribution in any medium, provided the original work is properly cited, the use is non-commercial and no modifications or adaptations are made.

The Madden-Julian Oscillation in a warmer world

Chiung-Wen June Chang[1], Wan-Ling Tseng[2], Huang-Hsiung Hsu[2], Noel Keenlyside[3], and Ben-Jei Tsuang[4]

[1]Department of Atmospheric Sciences, Chinese Culture University, Taipei, Taiwan, [2]Research Center for Environmental Changes, Academia Sinica, Taipei, Taiwan, [3]Geophysical Institute and Bjerknes Centre for Climate Research, University of Bergen, Bergen, Norway, [4]Department of Environmental Engineering, National Chung-Hsing University, Taichung, Taiwan

Abstract Global warming's impact on the Madden-Julian Oscillation (MJO) is assessed using one of the few models capable in reproducing its key features. In a warmer climate predicted for the end of the century, the MJO increases in amplitude (by ~30%) and frequency, showing a more circumglobal propagation tendency. The MJO spatial extent becomes enhanced, deeper, and more zonally extended but meridionally confined. A stronger vertical tilting structure in diabatic heating, moisture, and convergence fields is seen. Our findings indicate that these changes result from an intensification of the frictional wave-conditional instability of the second kind mechanism via the coupling of dynamical and thermodynamic response to the warming. The warming and moistening of the mean state contribute to the enhanced deep convective heating, driving a stronger-forced Kelvin wave-like perturbation. This reinforces the frictional low-level convergence, leading to larger shallow convective heating and therefore to a faster development and enhancement of the deep convection in the MJO.

1. Introduction

The Madden-Julian Oscillation (MJO) is the dominant pattern of atmospheric subseasonal variability in the tropics [*Madden and Julian*, 1971, 1972]. Despite its global importance, affecting monsoons, tropical storms, extratropical weather, the MJO is not well understood or simulated by state-of-the-art climate models [*Lin et al.*, 2006; *Kim et al.*, 2009; *Hung et al.*, 2013; *Jiang et al.*, 2015]. Thus, great uncertainty exists in how global warming will impact the MJO: the increase in atmospheric moisture content could intensify it [*Liu*, 2013; *Liu et al.*, 2013; *Schubert et al.*, 2013; *Subramanian et al.*, 2014; *Arnold et al.*, 2015], while atmospheric circulation changes could weaken and alter its frequency [*Jones and Carvalho*, 2011; *Maloney and Xie*, 2013; *Schubert et al.*, 2013].

Model and observational studies indicate that the MJO is strongly influenced by the mean state [*Maloney and Hartmann*, 2001; *Inness and Slingo*, 2003; *Zhang and Dong*, 2004; *Maloney and Xie*, 2013]. Perturbed sea surface temperature (SST) and large-scale flows patterns can impact MJO characteristics by changing wind shear, stability, moisture availability, and distribution. Thus, anthropogenic global warming will also likely impact the structure and behavior of the MJO. Limited number of available MJO projections show that MJO may amplify, and its variance increases appreciably with increasing warming [*Liu*, 2013; *Liu et al.*, 2013; *Schubert et al.*, 2013; *Subramanian et al.*, 2014; *Arnold et al.*, 2015]. The cause of the MJO amplification in these studies was attributed to an enhancement of the moisture mode by mean vertical advection of anomalous moisture static energy [e.g., *Arnold et al.*, 2015] and by strengthening the nonlinear wind-induced surface heat exchange mechanism [*Liu*, 2013]. However, the nonuniform increase in tropical SST under global warming may strongly modulate the changes [*Jones and Carvalho*, 2011; *Kang et al.*, 2013; *Maloney and Xie*, 2013].

Some of the aforementioned studies were conducted in idealized settings such as aquaplanet experiments, and some were conducted using models of weak MJO simulations. Thus, further investigation using models that better represent the MJO in more realistic configurations is necessary to explore the impact of global warming on the MJO. Here we use a new climate model, ECHAM5-SIT, which is the atmospheric general circulation model ECHAM5 coupled to a one-column turbulent kinetic energy ocean model Snow-Ice-Thermocline (SIT). ECHAM5-SIT is listed among the eight best models at simulating the MJO and four best at simulating convectively coupled wave spectra in a recent intercomparison of 27 models [*Jiang et al.*, 2015]. We compare the simulated MJO between a present and future time slice experiment, anticipating that ECHAM5-SIT may reliably represent MJO changes. We place the focus on characterization of the vertical structure of the MJO

during its life cycle. Thermodynamic and dynamic factors leading to the changes in the structure and propagation characteristics of the MJO are explored and presented.

2. Model and Time Slice Experimental Design

ECHAM5-SIT shows a markedly improved MJO simulation over the stand-alone ECHAM5 [*Roeckner*, 2003]. It is demonstrated that, by coupling SIT to ECHAM5, a better MJO can be simulated when the ocean-atmosphere interaction involving the upper few meters of the ocean is accurately represented [*Tseng et al*., 2014]. The one-column ocean model SIT describes changes in temperature, momentum, salinity, and turbulent kinetic energy driven by vertical fluxes parameterized using the classical K approach [*Tu and Tsuang*, 2005]. Extremely fine vertical resolution near the ocean surface enables SIT to simulate upper ocean temperature variations, such as the diurnal cycle, the few-millimeter thick cool skin layer at the ocean surface, and the warm layer beneath it. In our simulations, the coupled model is run with T63 (~1.8°) horizontal resolution, 31 vertical levels extending to 10 hPa (~30 km) in ECHAM5, and 42 vertical layers in SIT, with 12 in the upper 10 m. Active ocean-atmosphere interaction is allowed in the upper 10 m ocean via heat and momentum exchanges at every time step (12 min); the ocean below 10 m depth is weakly nudged to climatological monthly values to account for neglected horizontal processes. The coupling is only set in the tropics (30°S–30°N); elsewhere, monthly climatological SST and sea ice concentration (SIC) drive the AGCM. *Tseng et al*. [2014] provides a detailed description and sensitivity experiments of the model.

The present time slice experiment takes the observed 1981–2000 climatology for ocean temperature and salinity from Global Ocean Data Assimilation System [*Behringer and Xue*, 2004] and for SST and SIC from the Atmospheric Model Intercomparison Project II; the concentrations of greenhouse gases are fixed to values corresponding to the end of twentieth century. The SST, ocean temperature, and salinity conditions used in future time slice experiment are those of present plus the projected climatological changes for 2081–2100, relative to 1981–2000. The changes were derived from Max-Planck-Institute Earth System Model (MPI-ESM) historical and Representative Concentration Pathway 8.5 (RCP8.5) simulations performed for Coupled Model Intercomparison Project Phase 5 [*Giorgetta et al*., 2013]. The concentrations of greenhouse gases are fixed to the RCP8.5 values for the end of 21st century; for CO_2 this is about double the value in the present experiment. The SIC is set to the present-day observational value in both time slice experiments to isolate the influence of changes in the tropics. Influence of changing aerosol loading is also excluded by using the twentieth-century climatological values in both experiments. The analysis focuses on the boreal cool season (November–April), when this eastward-propagating equatorial phenomenon is most evident. The total simulation length of each experiment is 21 years, of which the last 20 years are used for analysis.

The MJO diagnosis tools used in this study are from the CLIVAR MJO Working Group, including the space-time filtering, the wave-frequency spectra, lag correlation diagram [*CLIVAR, M. J. O. W. G*, 2009], and the MJO index. The MJO signal is obtained by applying 20–100 day band-pass filtering to the observed and modeled daily data. MJO phase composites are computed, using the MJO index defined by the leading pair of principal components from an Empirical Orthogonal Function analysis of equatorial averaged (15°N–15°S) anomalies of outgoing longwave radiation, 850 and 200 hPa zonal winds [*Wheeler and Hendon*, 2004]. Each one of the eight distinct phases of the MJO index corresponds to a particular region where the deep convective envelope of the MJO is located. Temporal variation of vertical structure presented in this paper is demonstrated for the eight phases of the MJO cycle averaged over the Maritime Continent (120°–150°E, 10°S–0°N), so that the deep convective signal is centered between phase 4 and phase 5. As the MJO is an eastward-propagating phenomenon, the horizontal (phase) axis can be equivalently considered as the zonal direction [*Kim et al*., 2009].

3. Changes in Characteristics of the MJO

Compared to present, the future SST mean increases more than 2 K over the whole tropics, with the largest warming exceeding 3.6 K in the Maritime Continent and the Arabian Sea (Figure S1a in the supporting information). The increases in SST lead to a meridional broadening of the warmest SST region (50°E–180°E) and generally weaker SST gradients in the tropics (supporting information Figure S2a). The mean low-level westerly winds are enhanced and expanded slightly eastwards and northwards in the tropical Western Pacific but weakened slightly in magnitude in the Indian Ocean and the western Maritime Continent (supporting information Figure S1b). The easterlies in the Western Pacific from the equator to 10°N are largely weakened.

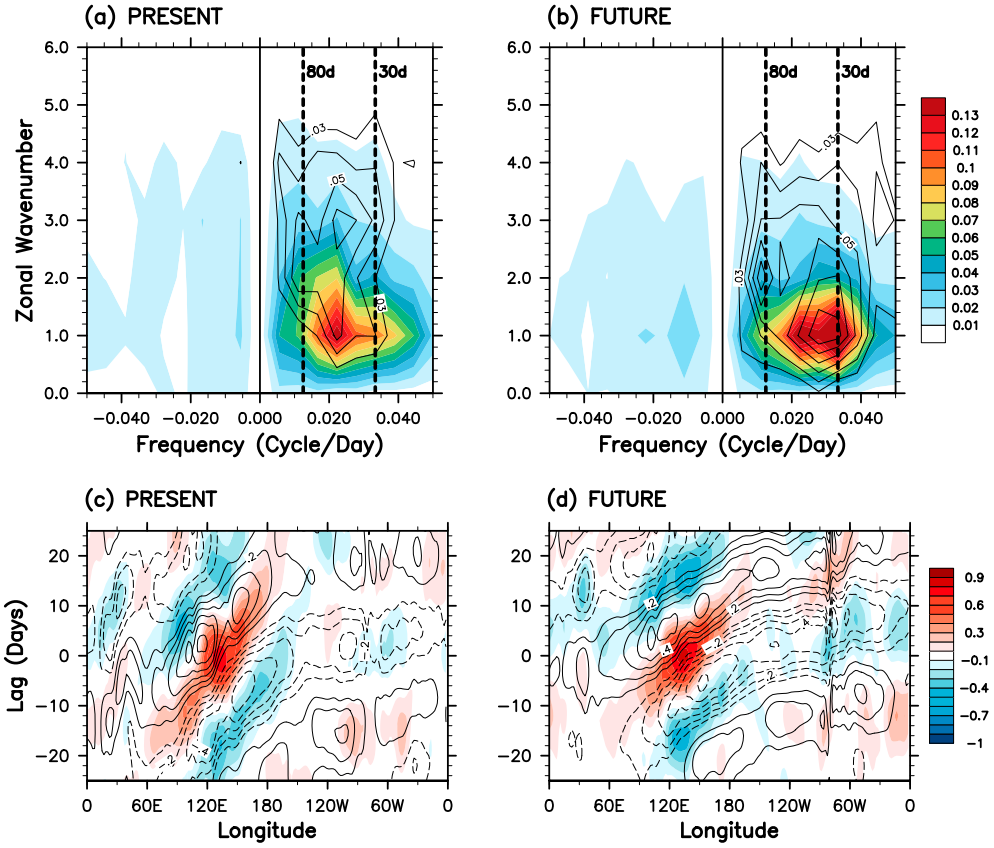

Figure 1. (a and b) The wave number-frequency spectra for equatorial 850 hPa zonal wind (shading) and precipitation anomalies (contour). Contour interval is 0.1 starting from value 0.3. (c and d) The lag-longitude diagrams of intraseasonal precipitation (shading) and 10 m zonal wind (contour) correlated against precipitation at region (10°S–0°N, 120°–150°E).

The mean precipitation and moisture are enhanced in the future experiment, as is the intraseasonal variance of precipitation (supporting information Figures S2b and S2c); this indicates a background with more abundant moisture supply and stronger convection and also more vigorous intraseasonal variability.

Figure 1 plots the wave number-frequency spectra of precipitation and 850 hPa zonal wind anomalies of the experiments. The present experiment demonstrates ECHAM5-SIT ability to produce realistic spectral characteristics and strength of eastward propagation at wave number 1 for zonal wind and wave numbers 1–4 for precipitation with period of 30–80 days (Figure 1a). In the future experiment, the MJO remains in the wave number 1 structure for zonal wind with an overall enhancement of spectral power on intraseasonal periods (Figure 1b, shading). The MJO precipitation variability in the future experiment, however, indicates remarkably enhanced concentration of power at wave number 1 (Figure 1b, contour). By integrating the wave number-spectral band between eastward zonal wave numbers 1–4 and periods of 20–90 days, we find that the MJO-scale precipitation amplitude increases significantly by 17.5% in the future experiment relative to the present, whereas the wind anomalies increase by merely 4.4%. The relationship of the precipitation and wind anomalies change matches the weak temperature gradient thermodynamic balance as discussed in *Maloney and Xie* [2013]. The discrepancy of the zonal wind and precipitation amplitude changes is modified by the background dry stability change, which increases ~16% in the future experiment (supporting information Table S1).

One emerging feature in Figure 1 is the larger amplitude at shorter intraseasonal periodicity (period less than 30 days), representing an enhancement of faster eastward-propagating components. The time-longitude evolution of precipitation and zonal wind anomalies (Figures 1c and 1d) clearly show that the MJO speeds up in the future experiment as the lag slope of the anomalies becomes less steep to the west of the dateline. The seemly continuous wind and precipitation anomaly signals east of the dateline in the Eastern

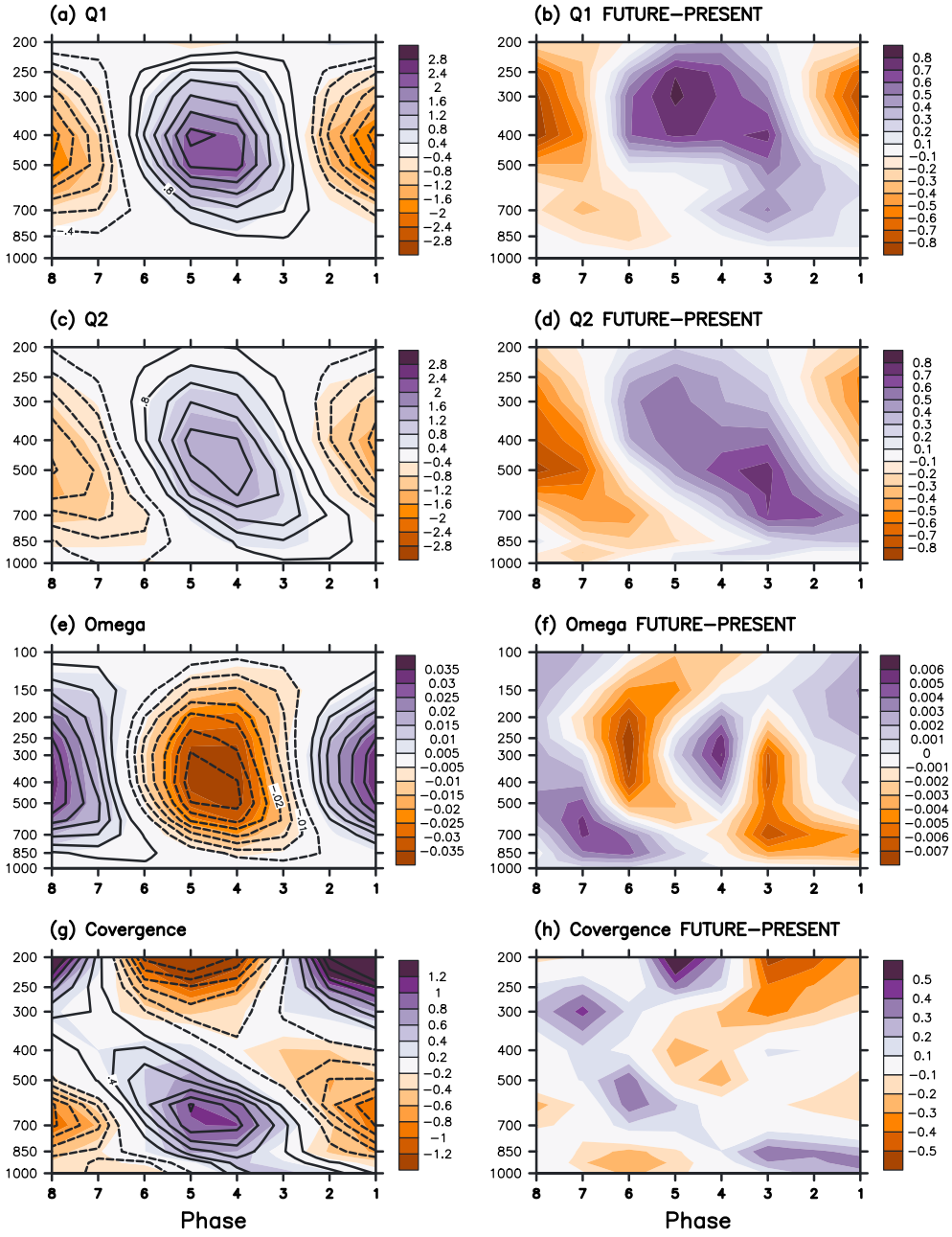

Figure 2. Vertical structure of the MJO in eight phases. (a, c, e, and g) Results from the present (shading) and the future (contour) experiments: (Figure 2a) diabatic heating ($W\,m^{-2}$), (Figure 2c) moisture sink ($W\,m^{-2}$), (Figure 2e) vertical velocity ($Pa\,s^{-1}$), (Figure 2g) horizontal convergence/divergence ($10^{-6}\,s^{-1}$). Contour intervals are the same as the shading intervals in Figures 2a, 2c, 2e, and 2g. (b, d, f, and h) Same as Figures 2a, 2c, 2e, and 2g but for the change relative to the present from the future experiment. Note that the convergence (divergence) is a positive (positive) value henceforth the warm (cold) colors in Figure 2c.

Pacific indicate that the future warming induces more circumglobal eastward-propagating perturbations in this region. The increase in propagation speed and circumglobal character is seen as increased power at 0.03–0.05 cycles per day and zonal wave number 1 in the supporting information Figure S5. This is part of an overall enhancement of the equatorial Kelvin waves in tropical wave spectra in the future experiment.

There are also key changes in the temporal evolution of vertical structure of the MJO, as shown by eight phase composites (Figure 2). The heating profile, calculated following the definition of Q_1 [*Yanai et al.*, 1973],

demonstrates a typical tropical maximum of diabatic heating at 500 hPa in the present experiment, whereas the maximum of heating in the future experiment is located higher in the troposphere around 400 hPa (Figure 2a). The heating increases largely in the future experiment from 500 hPa and above during the deep convective phases (phases 4 and 5), and there is a mild increase from 900 hPa to 500 hPa in the shallow convective phases (phases 1–3) (Figure 2b). The moisture sink profile, Q_2 [*Yanai et al*., 1973], illustrates an enhanced contribution of latent heating to the diabatic heating in the future experiment, starting from near the surface in phases 1 and 2, elevating to the middle troposphere in phase 3 and 4, and finally to the upper troposphere in phase 5 (Figures 2c and 2d). This temporal evolution indicates an enhanced westward-tilting structure in heating and moisture in the future experiment. The westward-tilting structure has been considered as an important ingredient in some MJO theories [*Kiladis et al*., 2005; *Zhang*, 2005; *Zhang et al*., 2013]. Temporal evolution of the moist static energy (MSE) also displays an enhanced westward-tilting structure in the future experiment (figure not shown).

In addition, we examine the vertical-integrated Q_1 from surface to 200 hPa which increases by about 26% in the deep convective phase in the future experiment (supporting information Figure S3). Correspondingly, the vertical-integrated Q_2 increases by about 33%. Thus, both Q_1 and Q_2 approximately follow Clausius-Clapeyron scaling, which would predict ~25% increase in moisture for the 3.5 K surface temperature increase. Moreover, the increases in Q_1 and Q_2 amplitude during phases 1–3 are accelerated by 34% and 37%, respectively, compared to the present experiment. Similarly, the amplitudes of negative Q_1 and Q_2 increase and the corresponding decrease during phases 5–7 are accelerated in the future experiment. The evolution of Q_1 and Q_2 shows that overall the future MJO may have an enhanced heating/cooling fluctuation.

The changes in MJO's dynamical fields show that low-level convergence and upward motion (omega) preceding MJO convection are enhanced (Figures 2f and 2h). This leads to increasing moistening of the boundary layer and contributes to the enhanced shallow heating in phases 1–3 (Figure 2b and supporting information Figure S4c). Overall, from phases 1–6 upward motion and convergence changes are enhanced and agree with the Q_1 profile, with the exception of the deep convective phases 4 and 5 when anomalous divergence and a reduction in omega above the midtroposphere occur. This seeming inconsistency between the heating and vertical motion/horizontal convergence will be explained later. Overall, the simulated changes in heating and omega indicate that the convection penetrates deeper into the troposphere in the future experiment, in concord with many model projections of an increased tropical convection depth under global warming scenarios [*Hartmann and Larson*, 2002; *Santer et al*., 2003; *Chou and Chen*, 2010; *Singh and O'Gorman*, 2012] and also with observational study [*Zelinka and Hartmann*, 2011].

Analysis of the MJO in phase 4 when deep convection is the strongest over the Maritime Continent shows the large-scale overturning zonal wind cell coupling to the convection (Figures 3a and 3b). In the future experiment, the positive heating region is significantly enlarged and deepened. Correspondingly, the convective-circulation envelope of the MJO is thicker and longitudinally wider as indicated by the circulation vectors. The stronger convection is associated with much enhanced low-level moisture convergence (green contour in Figures 3a and 3b). Furthermore, the rainfall in the future experiment becomes larger, and the sea level pressure (SLP) shows a more strongly meridionally confined and intensified Kelvin wave-like perturbation to the east of the deep convection (Figures 3e and 3f); this causes stronger low-level moisture convergence (not shown) consistent with the frictional wave-conditional instability of the second kind (CISK) mechanism [*Wang and Rui*, 1990; *Kang et al*., 2013]. By contrast, the meridionally overturning circulation is contracted meridionally toward an enhanced heating over 5°S (Figures 3c and 3d).

Results of the coupled and uncoupled experiments [*Tseng et al*., 2014] suggest that coupling leads to warmer SST and more moisture ahead of the deep convection. We diagnose the changes in moisture convergence between the two climate states since convection is related to the moisture source. The relative contribution of intraseasonal convergence and background moisture to the changes in moisture convergence in the future experiment is assessed as follows. Because the intraseasonal moisture convergence $-(\nabla \cdot q\mathrm{V})'$ is dominated by the MJO-scale convergence of the mean moisture, $-\overline{q}\,(\nabla \cdot \mathrm{V}')$ [*Hsu and Li*, 2012; *Tseng et al*., 2014], the changes in $\Delta\overline{q}\delta'_{\mathrm{CTL}}$ at each composite phase of the MJO cycle is diagnosed instead.

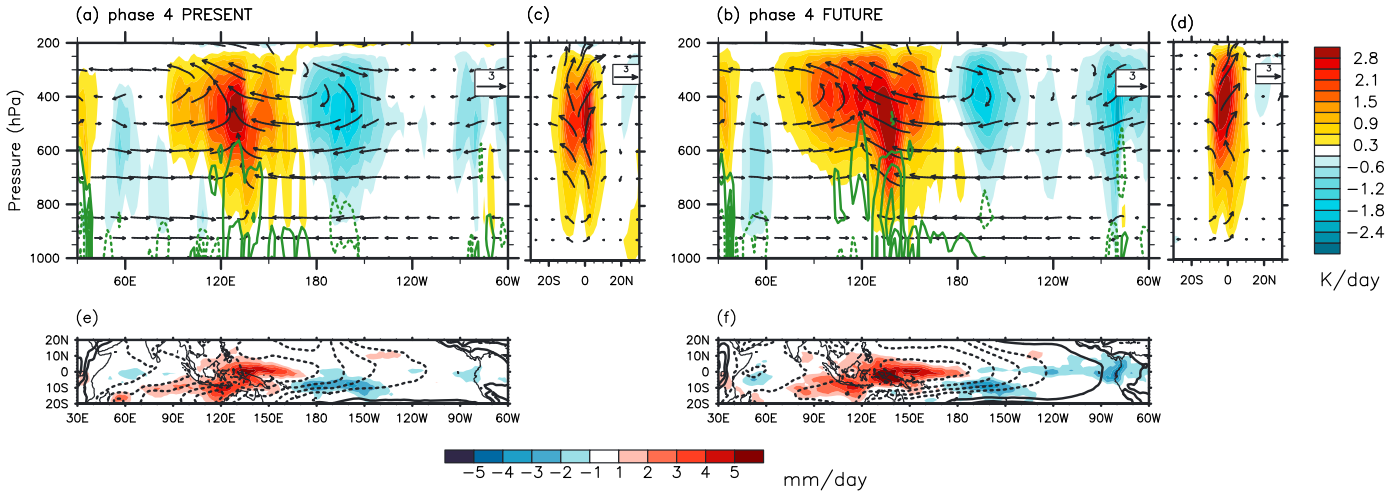

Figure 3. The longitude-height diagram (averaged over 10°S–0°N) and latitude-height diagram (averaged over 120°E–150°E) of the MJO scaled wind circulation (vector, u: m s^{-1}, omega: 10^{-2} Pa s^{-1}), Q_1 (shading, unit: W m^{-2}) and the horizontal moisture convergence (green contour, unit: 10^{-6} g kg^{-1} s^{-1}) for (a, c) present and (b, d) future. The contour interval of the moisture convergence is 8×10^{-6} g kg^{-1} s^{-1}; solid line is positive. Precipitation (shading, unit: mm d) and SLP (contour, unit: hPa) for (e) present and (f) future. Contour interval of SLP is 30 hPa; dash line is negative.

Overbar denotes the time mean and prime intraseasonal anomalies. For the sake of brevity, we use the notation δ' for the convergence $-\nabla \cdot \mathbf{V}'$. The changes in the MJO moisture flux convergence for future experiment relative to present can be written as

$$\underbrace{\Delta\left(\overline{q}\delta'\right)}_{a} = \underbrace{\overline{q}_{CTL}\Delta\delta'}_{b} + \underbrace{\left(\Delta\overline{q}\delta'_{CTL}\right)}_{c} + \underbrace{\left(\Delta\overline{q}\Delta\delta'\right)}_{d} \quad (1)$$

where Δ represents the future-present change and CTL denotes the present mean state. Equation (1) states that the change in moisture convergence relative to the current climate (term a) is associated with the change in the MJO flow convergence (term b), the change in background moisture (term c), and the nonlinear product of both background moisture and intraseasonal circulation changes (term d; which is a small term). The zonal-vertical distribution of terms a–c is plotted in shadings in Figures 4a–4c, respectively.

Relative to the present experiment, moisture convergence has marked increase centered at 700 hPa in phases 4–6 as well as near the surface in phases 1–3 (Figure 4a). Note the similarity to the westward tilting in Q_2 (Figure 2). The increase in moisture convergence centered at 700 hPa is indicative of a thicker

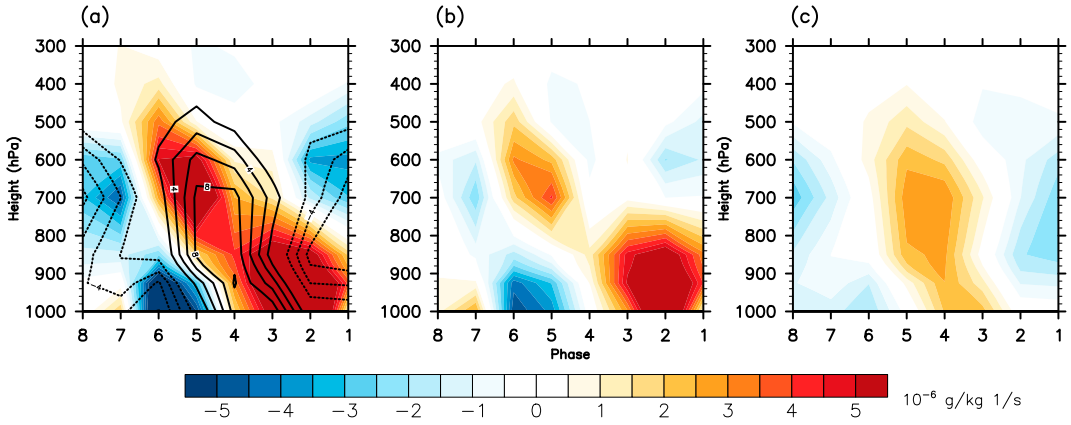

Figure 4. (a) Convergence of the mean moisture by the MJO flow ($\overline{q}\delta'$). Contour is the value in present run, shading plots the change relative to present ($\Delta(\overline{q}\delta')$). The contour interval is 2×10^{-6} g kg^{-1} s^{-1}; solid line is positive. (b) Convergence of the mean moisture by the MJO flow change ($\overline{q}_{CTL}\Delta\delta'$). (c) Convergence of the mean moisture by the mean background moisture change ($\Delta\overline{q}\delta'_{CTL}$). Note: negative contours and blue coloring denote the divergence, vice versa for the convergence.

moisture convergence layer in the lower troposphere in the future experiment, thus helping to foster higher and stronger deep convection. Nevertheless, the enhancement of moisture convergence in the future experiment may also be partially caused by the enhanced convection, as the two are closely coupled (as shown in Figure 3). Analysis shows that the 700 hPa moisture source increase can be attributed to both the change in MJO circulation ($-\overline{q}_{CTL}\Delta\delta'$, Figure 4b) and the background moisture ($\Delta\overline{q}\delta'_{CTL}$, Figure 4c). The increase in near-surface moistening is mainly dominated by the MJO dynamic change ($-\overline{q}_{CTL}\Delta\delta'$). Whereas the background moisture change enhances the main convection body observed in the present experiment, the dynamic change enhances the westward-tilting structure and the frictional moisture convergence [*Kiladis et al*., 2005; *Hsu and Li*, 2012], which moistens the boundary layer (up to about 850 hPa) ahead (east) of the deep convective clouds, resulting in a destabilized atmosphere favorable to the eastward movement of deep convection. The change in low-level moisture convergence to the east of the MJO deep convection is more than doubled from present to future, fractionally larger than the change in strength of MJO humidity change rate in the deep convective phase, which is about a 34% increase from present to future.

The seemingly inconsistent weakened circulation in the midtroposphere (Figure 2f) comparing with the enhanced Q_1 and Q_2 during phases 4 and 5 (Figures 2b and 2d) is explained as follows. The increased midtropospheric moisture convergence during phases 4 and 5 in the future experiment involves the increase in the background moisture (Figure 4c). Q_2 is therefore larger. A similar result is found in the estimation of Q_1: a weaker midtropospheric ascent in phases 4 and 5 is required to balance a diabatic heating anomaly under increased background dry stability change (supporting information Figure S4; also as explained in *Maloney and Xie* [2013]). In other words, the dynamical effect is overwhelmed by the thermodynamics effect in the midtroposphere during the deep convective phase of the MJO. In contrast, the enhancement of the near-surface preconditioning for the deep convection is contributed mostly by dynamical process.

4. Summary and Conclusion

The basic requirement for a future projection of the MJO is a climate model with a reasonable capability in simulating the MJO in current climate. Here we use a new climate model, ECHAM5-SIT, which ranks among the best models in MJO simulations [*Jiang et al*., 2015], anticipating reliably represented MJO changes. We compare the MJO between two climate states at the end of 20th and 21st century under the RCP8.5 high emissions scenario for its structure and propagation characteristics to infer the changes. In our simulations there is little change in the position of MJO activity under global warming. This is likely because the spatial distribution of low-level westerly and precipitation is hardly affected, although SST shows greater warming over the Indian Ocean compared to the eastern equatorial Pacific. Our results show that in a warmer climate, the MJO remains wave number 1 structure with a larger amplitude and greater eastward-propagating speed. The amplitude of precipitation increases by about 17% in future, while the zonal wind changes insignificantly. The small change in wind is due to the compensation effect of an increase in the background dry stability associated with warming (as discussed in *Maloney and Xie* [2013]).

In the tropics where the moist process dominates, the increased atmospheric moisture and temperature associated with global warming lead to larger MSE near the surface; the lower-level atmosphere tends to be more unstable as the equivalent potential temperature rate dropping more sharply with height below 500 hPa (figure not shown). This altered thermodynamic mean state leads to great enhancement of the MJO deep convection. The column integrated heat and moisture during the MJO deep convective phases increase by ~30%, leading to enhanced MJO heating/cooling. Spatially, the MJO circulation cell and deep convection become stronger and expand both vertically and zonally but more meridionally confined. In our simulation, the shallow heating preceding the deep convective heating is also enhanced. The significantly enhanced westward tilting with height in heating and moisture convergence fields is simulated because of the stronger low-level mass convergence. The strengthened MJO deep convection leads to a stronger equatorial Kelvin wave-like perturbation, which in turn reinforces low-level moisture convergence. Thus, the moistening process east of the deep convection is enhanced through the dynamical process.

We propose the following hypothesis: As the deeper convection resulting from a moister low-level background state excites stronger Kelvin waves, the enhanced moisture convergence leads to the more efficient and timely preconditioning of the deep convection and therefore to a faster development and

enhancement of the deep convection in MJO. In other words, it is an intensification of the frictional wave-CISK mechanism. The enhanced convection likely induces stronger Kelvin wave-like perturbations that propagate eastward across the relatively dry Eastern Pacific and enhances the circumglobal propagation tendency. Here we see that the key changes in the MJO vertical structure are closely associated with the mutual strengthening of thermodynamic and dynamic factors. It is nevertheless difficult to assess the cause and effect between the two.

The identification of a robust increase in MJO amplitude in a warmer climate presented here is consistent with several other recent studies. This result implies that the MJO is likely to exert larger impact on monsoons, tropical storms, extratropical weather, and the El Niño Southern Oscillation in the warming future. It is worth noting that, although the ECHAM5-SIT simulates the MJO reasonably well, the mechanisms for the MJO remain uncertain, and our results may represent only one aspect of the potential MJO changes under global warming. The intermodel spread in MJO changes is yet to be identified, and, for example, how dependent the projected changes are on the physical parameterization schemes, such as cumulus convection [*Zhou et al.*, 2012; *Ajayamohan et al.*, 2013; *Crueger et al.*, 2013], is an important issue that needs to be resolved. A systematic and well-designed series of MJO projection using various GCMs that realistically simulate this phenomenon is needed to identify the potential spread of the MJO changes in warming scenario.

Acknowledgments

ECHAME5-SIT data are available upon request by contacting the corresponding author. This work is supported by projects MOST 103-2111-M-034-004-, MOST 100-2119-M-001-029-MY5, and MOST 103-2621-M-005-003-. EU-STEPS (PCIG10-GA-2011-304243) project and Center for Climate Dynamics (SKD) provide mobility support for the work. NK acknowledges support from EU FP7 PREFACE project (grant agreement 603521). The authors thank P.-C. Hsu, T.Li, and C.-A. Chen for their helpful discussions. Computer time and facilities were provided by National Center for High-Performance Computing, Taiwan.

The Editor thanks two anonymous reviewers for their assistance in evaluating this paper.

References

Ajayamohan, R., B. Khouider, and A. J. Majda (2013), Realistic initiation and dynamics of the Madden-Julian Oscillation in a coarse resolution aquaplanet GCM, *Geophys. Res. Lett.*, *40*, 6252–6257, doi:10.1002/2013GL058187.

Arnold, N. P., M. Branson, Z. Kuang, D. A. Randall, and E. Tziperman (2015), MJO intensification with warming in the super-parameterized CESM, *J. Clim.*, *28*, 2706–2724, doi:10.1175/JCLI-D-14-00494.1.

Behringer, D., and Y. Xue (2004), Evaluation of the global ocean data assimilation system at NCEP: The Pacific Ocean, paper presented at Proc. Eighth Symp. on Integrated Observing and Assimilation Systems for Atmosphere, Oceans, and Land Surface.

Chou, C., and C.-A. Chen (2010), Depth of convection and the weakening of tropical circulation in global warming, *J. Clim.*, *23*(11), 3019–3030.

CLIVAR, M. J. O. W. G (2009), MJO simulation diagnostics, *J. Clim.*, *22*(11), 3006–3030.

Crueger, T., B. Stevens, and R. Brokopf (2013), The Madden–Julian Oscillation in ECHAM6 and the introduction of an objective MJO metric, *J. Clim.*, *26*(10), 3241–3257.

Giorgetta, M. A., J. Jungclaus, C. H. Reick, S. Legutke, J. Bader, M. Böttinger, V. Brovkin, T. Crueger, M. Esch, and K. Fieg (2013), Climate and carbon cycle changes from 1850 to 2100 in MPI-ESM simulations for the Coupled Model Intercomparison Project phase 5, *J. Adv. Model. Earth Syst.*, *5*, 572–597, doi:10.1002/jame.20038.

Hartmann, D. L., and K. Larson (2002), An important constraint on tropical cloud-climate feedback, *Geophys. Res. Lett.*, *29*(20), 1951, doi:10.1029/2002GL015835.

Hsu, P.-C., and T. Li (2012), Role of the boundary layer moisture asymmetry in causing the eastward propagation of the Madden-Julian Oscillation*, *J. Clim.*, *25*(14), 4914–4931.

Hung, M.-P., J.-L. Lin, W. Wang, D. Kim, T. Shinoda, and S. J. Weaver (2013), MJO and convectively coupled equatorial waves simulated by CMIP5 climate models, *J. Clim.*, *26*(17), 6185–6214.

Inness, P. M., and J. M. Slingo (2003), Simulation of the Madden-Julian Oscillation in a coupled general circulation model. Part I: Comparison with observations and an atmosphere-only GCM, *J. Clim.*, *16*(3), 345–364.

Jiang, X., et al. (2015), Vertical structure and physical processes of the Madden-Julian Oscillation: Exploring key model physics in climate simulations, *J. Geophys. Res. Atmos.*, *120*, 4718–4748, doi:10.1002/2014JD022375.

Jones, C., and L. Carvalho (2011), Will global warming modify the activity of the Madden–Julian Oscillation?, *Q. J. R. Meteorol. Soc.*, *137*(655), 544–552.

Kang, I.-S., F. Liu, M.-S. Ahn, Y.-M. Yang, and B. Wang (2013), The role of SST structure in convectively coupled Kelvin-Rossby waves and its implications for MJO formation, *J. Clim.*, *26*(16), 5915–5930.

Kiladis, G. N., K. H. Straub, and P. T. Haertel (2005), Zonal and vertical structure of the Madden-Julian Oscillation, *J. Atmos. Sci.*, *62*(8), 2790–2809.

Kim, D., K. Sperber, W. Stern, D. Waliser, I.-S. Kang, E. Maloney, W. Wang, K. Weickmann, J. Benedict, and M. Khairoutdinov (2009), Application of MJO simulation diagnostics to climate models, *J. Clim.*, *22*(23), 6413–6436.

Lin, J.-L., G. N. Kiladis, B. E. Mapes, K. M. Weickmann, K. R. Sperber, W. Lin, M. C. Wheeler, S. D. Schubert, A. Del Genio, and L. J. Donner (2006), Tropical intraseasonal variability in 14 IPCC AR4 climate models. Part I: Convective signals, *J. Clim.*, *19*(12), 2665–2690.

Liu, P. (2013), Changes in a modeled MJO with idealized global warming, *Clim. Dyn.*, *40*(3–4), 761–773.

Liu, P., T. Li, B. Wang, M. Zhang, J.-j. Luo, Y. Masumoto, X. Wang, and E. Roeckner (2013), MJO change with A1B global warming estimated by the 40-km ECHAM5, *Clim. Dyn.*, *41*(3–4), 1009–1023.

Madden, R. A., and P. R. Julian (1971), Detection of a 40–50 day oscillation in the zonal wind in the tropical Pacific, *J. Atmos. Sci.*, *28*(5), 702–708.

Madden, R. A., and P. R. Julian (1972), Description of global-scale circulation cells in the tropics with a 40–50 day period, *J. Atmos. Sci.*, *29*(6), 1109–1123.

Maloney, E. D., and D. L. Hartmann (2001), The Madden-Julian Oscillation, barotropic dynamics, and North Pacific tropical cyclone formation. Part I: Observations, *J. Atmos. Sci.*, *58*(17), 2545–2558.

Maloney, E. D., and S. P. Xie (2013), Sensitivity of tropical intraseasonal variability to the pattern of climate warming, *J. Adv. Model. Earth Syst.*, *5*, 32–47, doi:10.1029/2012MS000171.

Roeckner, E. (2003), *The Atmospheric General Circulation Model ECHAM5. Part 1: Model Description*, Max-Planck-Institut fuer Meteorologie, Hamburg, Germany.

Santer, B. D., M. F. Wehner, T. Wigley, R. Sausen, G. Meehl, K. Taylor, C. Ammann, J. Arblaster, W. Washington, and J. Boyle (2003), Contributions of anthropogenic and natural forcing to recent tropopause height changes, *Science*, *301*(5632), 479–483.

Schubert, J. J., B. Stevens, and T. Crueger (2013), Madden-Julian Oscillation as simulated by the MPI Earth System Model: Over the last and into the next millennium, *J. Adv. Model. Earth Syst.*, *5*, 71–84, doi:10.1029/2012MS000180.

Singh, M. S., and P. A. O'Gorman (2012), Upward shift of the atmospheric general circulation under global warming: Theory and simulations, *J. Clim.*, *25*(23), 8259–8276.

Subramanian, A., M. Jochum, A. J. Miller, R. Neale, H. Seo, D. Waliser, and R. Murtugudde (2014), The MJO and global warming: A study in CCSM4, *Clim. Dyn.*, *42*(7–8), 2019–2031.

Tseng, W.-L., B.-J. Tsuang, N. Keenlyside, H.-H. Hsu, and C.-Y. Tu (2014), Resolving the upper-ocean warm layer improves the simulation of the Madden–Julian Oscillation, *Clim. Dyn.*, *1–17*, doi:10.1007/s00382-014-2315-1.

Tu, C. Y., and B. J. Tsuang (2005), Cool-skin simulation by a one-column ocean model, *Geophys. Res. Lett.*, *32*, L22602, doi:10.1029/2005GL024252.

Wang, B., and H. Rui (1990), Dynamics of the coupled moist Kelvin-Rossby wave on an equatorial-plane, *J. Atmos. Sci.*, *47*(4), 397–413.

Wheeler, M. C., and H. H. Hendon (2004), An all-season real-time multivariate MJO index: Development of an index for monitoring and prediction, *Mon. Weather Rev.*, *132*(8), 1917–1932.

Yanai, M., S. Esbensen, and J.-H. Chu (1973), Determination of bulk properties of tropical cloud clusters from large-scale heat and moisture budgets, *J. Atmos. Sci.*, *30*(4), 611–627.

Zelinka, M. D., and D. L. Hartmann (2011), The observed sensitivity of high clouds to mean surface temperature anomalies in the tropics, *J. Geophys. Res.*, *116*, D23103, doi:10.1029/2011JD016459.

Zhang, C. (2005), Madden-Julian Oscillation, *Rev. Geophys.*, *43*, RG2003, doi:10.1029/2004RG000158.

Zhang, C., and M. Dong (2004), Seasonality in the Madden-Julian Oscillation, *J. Clim.*, *17*(16), 3169–3180.

Zhang, C., J. Gottschalck, E. D. Maloney, M. W. Moncrieff, F. Vitart, D. E. Waliser, B. Wang, and M. C. Wheeler (2013), Cracking the MJO nut, *Geophys. Res. Lett.*, *40*, 1223–1230, doi:10.1002/grl.50244.

Zhou, L., R. B. Neale, M. Jochum, and R. Murtugudde (2012), Improved Madden-Julian Oscillations with improved physics: The impact of modified convection parameterizations, *J. Clim.*, *25*(4), 1116–1136.